

Engineering spin-waves in a high-spin ultracold Fermi gas

J. Heinze¹, J. S. Krauser¹, N. Fläschner¹, K. Sengstock^{1,2,*}, and C. Becker^{1,2}

¹*Institut für Laser-Physik, Universität Hamburg, Luruper Chaussee 149, 22761 Hamburg, Germany*

²*Zentrum für Optische Quantentechnologien, Universität Hamburg, Luruper Chaussee 149, 22761 Hamburg, Germany*

U. Ebling³, A. Eckardt⁴, and M. Lewenstein^{3,5}

³*ICFO - Institut de Ciències Fotòniques, Av. Carl Friedrich Gauss, 3, 08860 Castelldefels (Barcelona), Spain*

⁴*Max-Planck-Institut für Physik komplexer Systeme, Nöthnitzer Str. 38, 01187 Dresden, Germany*

⁵*ICREA-Institució Catalana de Recerca i Estudis Avançats, Lluís Companys 23, 08010 Barcelona, Spain*

We report on the detailed study of multi-component spin-waves in an $s=3/2$ Fermi gas where the high spin leads to novel tensorial degrees of freedom compared to $s=1/2$ systems. The excitations of a spin-nematic state are investigated from the linear to the nonlinear regime, where the tensorial character is particularly pronounced. By tuning the initial state we engineer the tensorial spin-wave character, such that the magnitude and sign of the counterflow spin-currents are effectively controlled. A comparison of our data with numerical and analytical results shows excellent agreement.

PACS numbers: 05.30Fk, 03.75Ss, 75.30Ds

Spin-interaction driven phenomena are crucial for the behavior of many quantum systems, e.g., ferromagnets [1] and high-temperature superconductors [2] and are also relevant in spintronics applications [3]. Apart from condensed matter systems with an electronic spin of $s=1/2$, dilute atomic gases show a wealth of novel spin-excitations, where the spin is provided by the internal hyperfine structure of the atoms. Pioneering experiments with hydrogen [4] and helium [5] showed the existence of transversal spin-waves, which arise from intrinsic spin-exchange interactions [6–8]. Longitudinal spin-waves in two-component mixtures have been demonstrated in non-condensed bosonic ^{87}Rb [9]. For weakly interacting fermions, slow spin-currents were reported near the zero-crossing of a Feshbach-resonance [10] and the interaction-induced damping of dipole oscillations was studied [11]. Prominent examples for strongly interacting fermionic systems are the BEC-BCS crossover [12], miscibility of spin mixtures [13], and the quest for itinerant ferromagnetism [14–17]. In contrast to conventional two-component systems, the hyperfine structure of many atoms also allows for spinor gases with $s>1/2$, which offer a whole new set of possibilities to study spin-dependent phenomena [18, 19]. This includes the existence of spin-nematic states [20, 21], spin-changing collisions [22, 23], spontaneous domain formation [24], $\text{SU}(N)$ degenerate ground states [25–29], and novel superfluid phases [30, 31]. Especially for fermionic atoms, $s=3/2$ constitutes the simplest realization of a high-spin system and is thoroughly studied theoretically, being a model system for all higher spins [32, 33].

In this Letter, we investigate tunable spin-waves in a Fermi gas with pseudo-spin $s=3/2$ in the quantum degenerate regime, which constitute fundamental collective excitations in these systems. Spin-waves in such

high-spin systems are predicted to exhibit very complex and novel properties (see Refs. [34, 35] for bosonic systems): Higher spins require additional tensor components in addition to the well-known spin-vector used to describe $s=1/2$ system, such as nematic and octupole operators in the case of $s=3/2$. The coupling between these tensor components strongly influences the spin-wave properties and leads to completely new phenomena. We have investigated spin-wave excitations ranging from the linear regime, where only spatial dipole excitations are present to the non-linear regime, where the nematic spin-component predominantly couples to the quadrupolar spatial mode. The change of the spin-wave composition is accompanied by a change of the oscillation frequency, which has a minimum in the linear regime. In a second set of experiments, we engineer the initial state coherences. By this, the spin-current for two of the four components can be reversed changing the spin-wave character from spin-octupole to spin-vector. All results are in excellent agreement with numerical calculations based on a semiclassical mean-field theory (SMFT; a collisionless Boltzmann equation with full spin coherence) [35–38]. Our results demonstrate the high degree of control that can be exerted on spin-waves in high-spin Fermi gases and thus pave the way towards novel schemes for atom spintronics using the intrinsic high spin.

Our measurements are performed in a quantum degenerate gas of ^{40}K in the $f=9/2$ hyperfine manifold. We initially evaporate a balanced mixture of $|m=1/2\rangle$ and $|m=-1/2\rangle$ to quantum degeneracy in an optical dipole trap [36]. The final trapping frequencies are $\omega_{x,y,z}=2\pi \times (70, 70, 12) \text{ Hz}$. At this point, we apply a radio-frequency (rf) pulse to create a coherent superposition with the states $|\pm 3/2\rangle$ [Fig. 1(a)]. We initialize the spin-waves by applying a small magnetic field gradient up

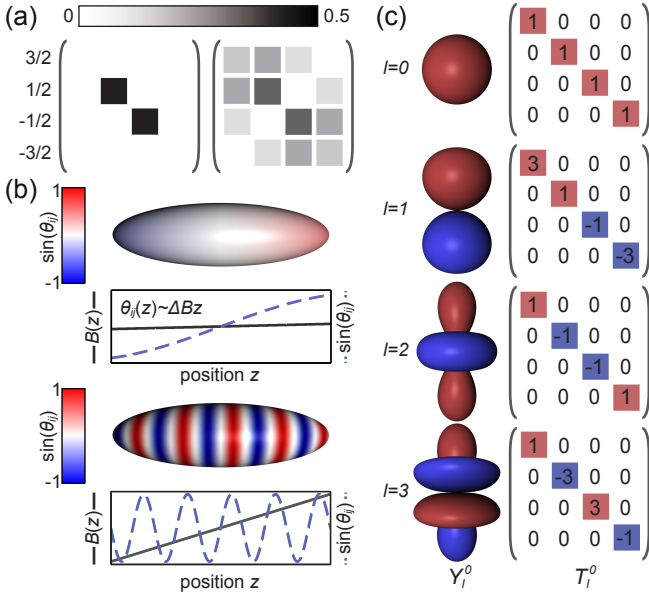


FIG. 1. (a) Single-particle density matrix for an incoherent superposition of $|1/2\rangle$ and $|-1/2\rangle$ (left) and the resulting coherent superposition of all four components after a resonant rf-pulse (right). Diagonal elements W_{ii} are real and represent the populations. Off-diagonal elements are complex numbers $W_{ij} = |W_{ij}|e^{i\theta_{ij}}$ and include the phase θ_{ij} between different components. Plotted is only the absolute value $|W_{ij}|$ (b) Sketch of the local phase across the Fermi gas after pulses with different magnetic field gradients. (c) $m=0$ component of the $l=0,1,2,3$ tensor operators T_l^m for $s=3/2$ in comparison to the corresponding spherical harmonics Y_l^m .

to a few G/m for 10 ms, which leads to a phase spiral for coherent superpositions of different spin-components as sketched in Fig. 1(b). While these coherent superpositions are initially still spin-polarized locally, the phase-twist allows for interactions in a trapped gas where the external potential induces spatial dynamics [37]. In general, the resulting mean-field interaction couples the spin degrees of freedom to different modes of the external trap leading to the emergence of spin-waves. We detect the spin-current using absorption imaging either *in situ* or after 18.5 ms time-of-flight (TOF) with a Stern-Gerlach separation of the spin-components [36]. In Fig. 2(a) we show a typical example for a $s=3/2$ spin-wave initialized by a 10 ms gradient of $\Delta B = 3.4$ G/m. The measurements reveal oscillatory spin-currents in all four spin-components. We observe a time-independent total density, meaning that these spin-waves constitute counter-flow spin-currents without an accompanying net mass transport. In particular, note the inverted flow direction of $|1/2\rangle$ ($|-1/2\rangle$) with respect to the $|3/2\rangle$ ($|-3/2\rangle$), which is a clear indication of the new tensorial degrees of freedom as discussed later.

Let us at this point introduce a description of spin in the language of tensors which transform invariant under rotations, to obtain a deeper insight into the underlying

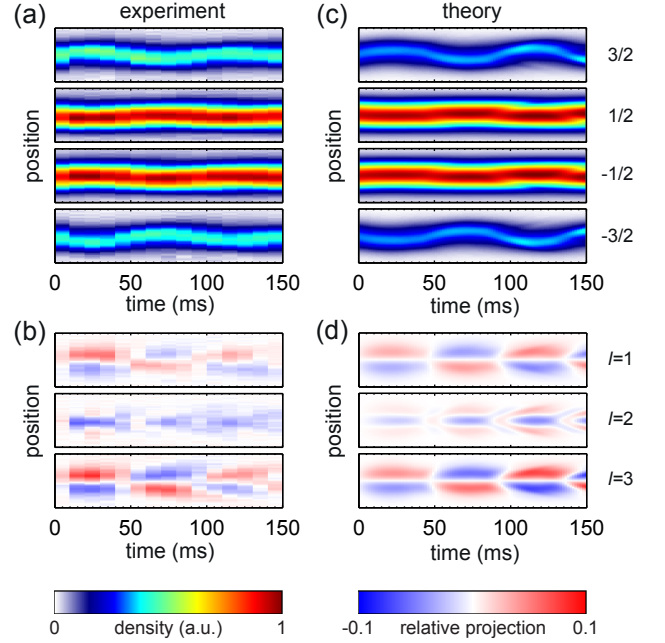


FIG. 2. (a) *In situ* time evolution of all four spin-components after a 10 ms pulse with a magnetic field gradient of $\Delta B = 3.4$ G/m. Shown are the column densities at different times after the excitation. (b) Deviation from the initial population of the $m=0$ component of the vector ($l=1$), nematic ($l=2$) and octupole ($l=3$) component. The vector and octupole component show spatial dipole oscillations, while the nematic component clearly exhibits quadrupolar spatial oscillations. (c,d) Numerical calculation for the parameters of (a,b).

physical processes. Most common are the spherical harmonics for orbital angular momentum [Fig. 1(c)] and the spin-vector $\vec{S} \propto (\sigma_x, \sigma_y, \sigma_z)$ where σ_i are the Pauli matrices. The latter are conveniently used as a basis set to describe any (pseudo) $s=1/2$ system. To describe the physics of larger spins, however, it is necessary to include higher order tensors. In a spin $3/2$ system, as discussed here, in addition to the spin-vector ($l=1$), the spin-nematic tensor ($l=2$) and the spin-octupole tensor ($l=3$) must be included (see Fig. 1(c) and [36]). In particular, this basis set automatically fulfills all possible rotation symmetries which simplify the equations of motion. The initial state in Fig. 2 is explicitly chosen to be purely nematic to exploit these symmetries in the experiments. The time evolution of the $l=1,2,3$ tensors for the measurements of Fig. 2(a) is shown in Fig. 2(b). Note the predominantly quadrupolar spatial dynamics of the spin-nematic component, qualitatively different from the dipolar oscillations in the spin-vector and spin-octupole component. This results from a self-decoupling of the nematic component due to the rotational symmetry and our properly chosen initial state, as explained later.

High-spin spin-waves can be theoretically treated within SMFT [34–36]. In the tensor notation, this is

a generalization of the usual spin-vector approach for $s = 1/2$ systems [10, 37–40], which allows to understand the intriguing observations from Fig. 2. The system is described by a single-particle Wigner function $W(z, p)$ in one spatial dimension and the equation of motion takes the form of a Boltzmann-equation in the collisionless regime. To zeroth order in the SMFT one gets for a $s = 3/2$ gas in a spin-independent external harmonic trap

$$\partial_t W(z, p) = \partial_0 W(z, p) + \frac{1}{i\hbar} [W(z, p), V(z)]. \quad (1)$$

Here, $V_{mn}(z) = \int \sum_{kl} (U_{klmn} - U_{kmnl}) W_{kl}(z, p) dp$ is the effective mean-field interaction with the spin-dependent coupling constants U_{ijkl} [36], $\partial_0 = (-p/m\partial_z + m\omega_z^2 z\partial_p)$ captures the time evolution due to the harmonic trap and kinetic energy, m is the mass of ^{40}K , and $[\cdot, \cdot]$ indicates the commutator in spin space. In the simulations, also the first order gradient expansion in the interactions are taken into account, leading to very small deviations only [36]. For a $s = 3/2$ system, the Wigner function in spin space is a 4×4 single-particle density matrix (SPDM), where the diagonal elements W_{ii} represent the absolute population of the spin-components and the off-diagonal elements $W_{ij} = |W_{ij}|e^{i\theta_{ij}}$ represent the single-particle-coherences between different components. To induce a time evolution of the populations W_{ii} , it is sufficient to spatially vary the phases θ_{ij} of the off-diagonal elements W_{ij} , since they are coupled via the commutator in (1).

The equation of motion (1) can be cast into the tensor notation introduced above by decomposing the Wigner function (mean-field potential) into tensor components $W_1(V_1)$ [41]:

$$\begin{aligned} \partial_t W_0 &\cong \partial_0 W_0, \\ \partial_t W_1 &\cong \partial_0 W_1 + \frac{1}{i\hbar} ([W_1, V_1] + [W_2, V_2] + [W_3, V_3]), \\ \partial_t W_2 &\cong \partial_0 W_2 + \frac{1}{i\hbar} ([W_2, V_1 + V_3] + [W_1 + W_3, V_2]), \\ \partial_t W_3 &\cong \partial_0 W_3 + \frac{1}{i\hbar} ([W_3, V_1] + [W_1 + W_3, V_3] + [W_2, V_2]). \end{aligned} \quad (2)$$

The structure of (2) leads to several important consequences. First, the total density W_0 is not affected by the phase spiral, since it contains no off-diagonal elements. Therefore, the total density remains constant as we observe in the experiment. Second, the dynamics of the nematic tensor W_2 is proportional to the vector and octupole components (W_1 and W_3), while the latter two have terms proportional solely to the nematic $l = 2$ component. A purely nematic initial state as in Fig. 2 does therefore not support nematic excitations to first order. In the highly nonlinear regime, where vector and octupole excitations possess a large amplitude, nematic excitations are created via higher-order processes. This leads to the

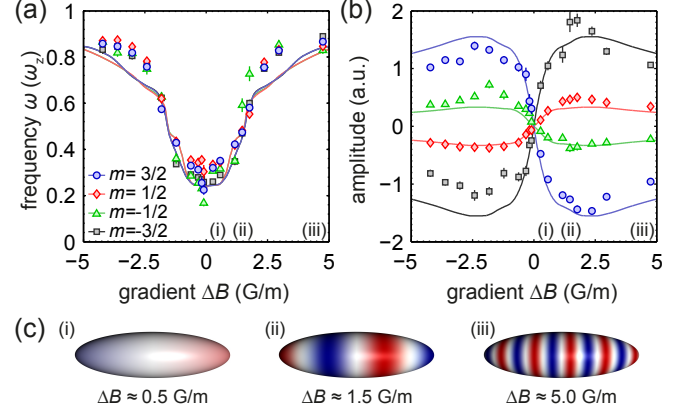


FIG. 3. (a) Frequency and (b) oscillation amplitude of spin-waves excited with different magnetic field gradients at $\omega_z = 12$ Hz. Negative amplitudes denote an inverted initial direction. Solid lines are numerical data for each component. All error bars solely correspond to fit errors, representing one standard deviation. The experimental amplitudes which are taken after TOF and the numerical amplitudes calculated *in situ* are rescaled onto each other by a global factor. (c) Sketch of the phase windings across the atom cloud for different gradient pulses.

spatially quadrupolar dynamics of the nematic component, which is qualitatively different from the spatially dipolar oscillations of the vector and octupole component [Fig. 2(b)]. Figure 2(c,d) show numerical results using (1) for the exact experimental parameters. Note, that these are in excellent agreement with the experimental results demonstrating the capability to understand complex spin-waves via the demonstrated tensorial spin-decomposition.

To analyze the behavior of the system for different excitation amplitudes, we applied different gradient strengths during the initialization of the spin-wave [42]. This corresponds to a change of the initial phases θ_{ij} in the SPDM, while the initial coherence amplitudes $|W_{ij}|$ are kept constant. In Fig. 3 experimental results are compared to numerical calculations and show very good agreement: For small gradients, the frequency is amplitude-independent and the amplitude rises approximately linear with the gradient strength. For large gradients, the frequency approaches the trapping frequency and is again only weakly depending on the excitation amplitude. For intermediate gradients, the system behaves strongly nonlinear which results in an amplitude-dependent oscillation frequency. In the regime of small gradients, corresponding to small excitation strengths one can apply the method of moments [43] up to linear order in z and p , which describes pure spatial dipole oscillations [36]. Their oscillation frequency for the present initial state can be derived to be $\omega = \sqrt{\omega_{\text{mf}}^2 + \omega_z^2} - \omega_{\text{mf}}$, where ω_{mf} is the mean-field interaction energy as defined in Ref. [36]. This frequency is determined by a competition between the trap induced spa-

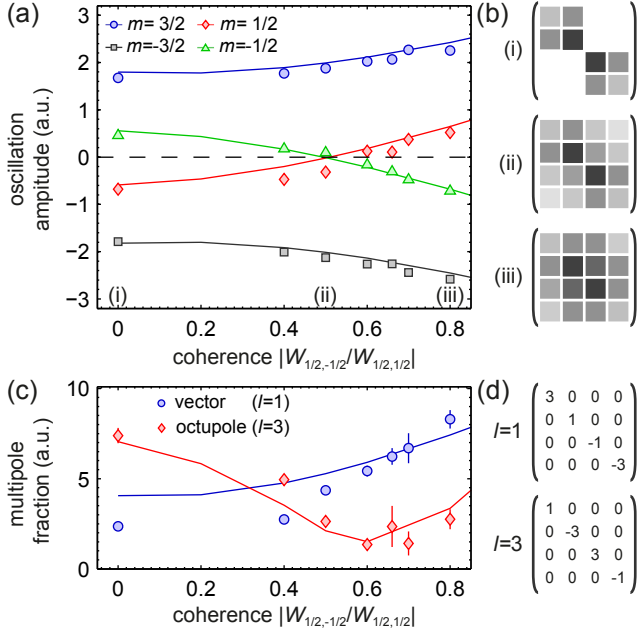


FIG. 4. (a) Spatial oscillation amplitude of the spin-wave excitations for different initial coherences but equal populations of the four components at $\Delta B = 3.6$ G/m. Solid lines show the initial spin-wave amplitude extracted from numerical calculations. (b) Exemplary SPDMs for different initial coherences. (c) Amplitude of the dipole and octupole tensor components [36]. (d) Vector and octupole tensors evaluated in (c). All error bars solely correspond to fit errors, representing one standard deviation. The experimental amplitudes which are taken after TOF and the numerical amplitudes calculated *in situ* are rescaled onto each other by a global factor.

tial oscillations and the mean-field rotation of the spin. For our parameters, we calculate $\omega = 2\pi \times 2.3$ Hz in good agreement with the experimental results. The linearized equations of motion also confirm the pure vector and octupole character of the dipole excitations for a perfectly nematic initial state as discussed above.

For large gradients, the frequency slowly approaches the trapping frequency: In this regime, the phase spiral only leads to an initial strong kick but is averaged out dynamically on timescales $2\pi/\omega_z$ [37]. Consequently, the mean-field potential no longer affects the subsequent oscillation and the corresponding frequency approaches the trap frequency with increasing winding number of the phase spiral, equivalent to an increasing gradient.

All measurements discussed so far were performed with the same purely nematic initial state. By modifying the rf-pulse sequences used for the preparation of the initial state we can control the amplitude of the coherences $|W_{ij}|$ and populations W_{ii} in the SPDM. By this the multipole decomposition of the initial state can be widely tuned and allows for the initialization of e.g. pure vector or nematic initial states, which in turn results in different spin and spatial characteristics of the emerging spin-

wave. Following this direction, we performed a second set of experiments, where we engineered the spin-wave excitations by keeping the population of all four spin-components constant but changing the initial coherence amplitudes $|W_{ij}|$ [Fig. 4(b)]. Note, that this is complementary to the results shown in Fig. 3, where we changed the phase θ_{ij} of the coherence by using different gradient strengths. Figure 4(a) shows the resulting oscillation amplitude for all four spin-components depending on $c = |W_{1/2,-1/2}/W_{1/2,1/2}|$. At $c \approx 0.5$ the system changes its qualitative behavior where the $|\pm 1/2\rangle$ components interchange their oscillation direction. Using the tensor notation, the spin-wave at small c is dominated by the spin-octupole, where neighboring spin-components have an inversed sign and therefore oscillate in opposed directions. At large c , the oscillation becomes spin-vector dominated, where spin-components with the same sign of magnetization oscillate in the same direction [Fig. 4(c)]. The anew increase of the octupole amplitude at large c is due to higher order spatial excitations, possible in the nonlinear regime, where the measurements were performed. At $c \approx 0.5$, the vector and octupole component contributions mutually cancel, leading to a vanishing spin-current in the $|\pm 1/2\rangle$ components. Again the numerical calculations describe the engineered spin-waves very well.

In conclusion, we have thoroughly investigated the physics of tunable spin-waves in a high-spin Fermi gas. We have generalized the spin-vector description of $s = 1/2$ systems by introducing higher order spin-tensors and used the corresponding decomposition of the equations of motion to explain the novel emerging spin-wave characteristics in a high-spin system. In particular, we observe a self-decoupling of the spin-nematic component, suppressing nematic spin-waves. Further, we have analyzed the spin-wave excitation spectrum for different phase spirals, corresponding to different excitation strengths ranging from the linear deep into the nonlinear regime. Finally, we demonstrated how to control the multipole character of spin-waves which leads to a reversal of the resulting counterflow spin-current of two spin-components. Our results constitute the first study of collective spin-spatial excitations in high-spin bulk Fermi gases and demonstrate the controlled manipulation of atomic spin-currents. This paves the way towards novel schemes for spintronics in ultracold atomic gases, using the intrinsic high spin as a valuable resource.

We acknowledge financial support by DFG via Grant No. FOR801, from Spanish MICINN (FIS 2008-00784, AAIL-Hubbard, FPI-fellowship), ERC grant QUAGATUA and the Spanish foundation universidad.es.

SUPPLEMENTAL INFORMATION

In this supplemental material we discuss the preparation of our fermionic quantum gas (S1), the detection after TOF and *in situ* (S2) and the data analysis (S3). The theoretical model is introduced in (S4) and the linearized calculation is presented in (S5). For the tensor expansion in the $s=3/2$ system see (S6).

S1. PREPARATION OF FERMIONIC QUANTUM GASES

We sympathetically cool about $N=2 \times 10^6$ spin-polarized ^{40}K atoms in the state $f=9/2$ and $|m=9/2\rangle$ to $0.1 T_F$ using ^{87}Rb in a magnetic trap. Afterwards we transfer the atoms to a crossed circular-elliptical optical dipole trap with $\lambda=812\text{ nm}$. The $1/e^2$ radii are $w_{x,y}=120\text{ }\mu\text{m}$ for the circular beam and $w_x=70\text{ }\mu\text{m}$ and $w_z=280\text{ }\mu\text{m}$ of the elliptical beam, where the tight focus is in the vertical direction. Using rf-pulses and rf-sweeps, an equal mixture of two the hyperfine states $|1/2\rangle$ and $|-1/2\rangle$ is prepared and evaporatively cooled in the trap by a 2 s exponential intensity ramp. The final trapping frequencies are typically $\omega_{x,y,z}=2\pi \times (70, 70, 12)\text{ Hz}$ with $N=3.5 \times 10^5$ particles at $0.25 T_F$.

S2. DETECTION AND ANALYSIS OF SPIN COMPONENTS

To obtain the experimental data, we used two different detection protocols, which have complementary advantages. In most of the experiments, we applied time of flight imaging, where we switch off all optical potentials, and perform a Stern-Gerlach separation of the different spin states within the free expansion time of 18.5 ms. The atoms are detected via resonant absorption imaging and the center-of-mass is calculated for each of the separated clouds individually. This method has the advantage that all spin-components can be detected simultaneously, but the disadvantage that all spatial modes but the dipole mode are effectively washed out, since the TOF mixes momentum and spatial components of these modes.

To obtain more information on the spatial modes of the excited spin-waves we employed an *in situ* detection protocol, allowing us to observe, e.g., the quadrupole oscillations in Fig. 2(b). Instead of separating the different spins by a Stern-Gerlach procedure in TOF, we use microwave pulses at 1.3 GHz, to transfer all but one single component to the $f=7/2$ manifold of ^{40}K , which is off-resonant to the detection light, and consequently the transferred atoms do not appear in the absorption images. Afterwards we switch off all magnetic fields and optical potentials for 1 ms to detect the atomic sample.

To record the time evolution of all four components, it is therefore necessary to repeat the full measurement four times.

S3. ANALYSIS OF EXPERIMENTAL DATA

For every time step of the spin-wave dynamics, we determine the center-of-mass of each of the spin components. We extract the oscillation frequencies ω by fitting an exponentially damped cosine of the form

$$\text{COM}(t) = A \exp(-\Gamma t) \cos(\omega t + \Phi) + C, \quad (3)$$

with oscillation amplitude A , damping rate Γ , a phase shift Φ and a constant offset C . For the dipole and octupole fraction in Fig. 4(c), we use a slightly different method. We take the spatial average of the absolute value of the projected multipoles M for each time step as

$$M(t) = \frac{1}{N_p} \sum_p |M(p, t)| \quad (4)$$

where p is the pixel index of the image and N_p is the number of pixels. By this procedure, the sign-informations of the projection are lost and therefore, we fit the resulting time series by

$$M(t) = A \exp(-\Gamma t) \cos(\omega t + \Phi)^2 + C \quad (5)$$

and report the amplitude A .

S4. KINETIC EQUATION FOR A TRAPPED HIGH SPIN FERMI GAS

We describe the multi-component fermionic system using the single-particle Wigner-function, with its time evolution given by the semiclassical kinetic equation

$$\begin{aligned} \partial_t W(z, p) = \partial_0 W(z, p) + \frac{1}{i\hbar} [W(z, p), V(z)] \\ + \frac{1}{2} \{ \partial_p W(z, p), \partial_z V(z) \} \end{aligned} \quad (6)$$

with the short notation $\partial_0 \equiv -\frac{p}{m} \partial_z + m\omega_z^2 z \partial_p$ for the single-particle part of motion. We do not explicitly include the magnetic field gradient, since it is used for the creation of the spin-wave but not necessary for its propagation once created. The derivation of this equation is outlined in previous works [37, 38]. One basically starts from the full mean-field dynamics of the Wigner function and applies a semiclassical approximation by neglecting terms involving higher order derivatives with respect to position and momentum. To leading (zeroth) order, the mean-field interaction gives rise to the commutator and the next (first) order is given by the anticommutator. We have neglected here even higher orders terms. The

important term here is the commutator which is absent in the spinless case and describes interaction driven coherent spin dynamics. It is also dominant with respect to the anticommutator and we neglect the latter in our analytical studies (while we keep it in the numerical simulations). The kinetic equation (6) is nonlinear, since the mean-field potential depends on the Wigner-function itself and its matrix elements are defined as

$$V_{mn}(z) = \int dp \sum_{kl} (U_{klmn} - U_{kmnl}) W_{kl}(z, p) \quad (7)$$

with the coupling constants defined as $U_{ijkl} = \sum_{S=0,2,\dots}^{2s-1} g_S \sum_{M=-S}^S \langle SM|ik\rangle \langle SM|jl\rangle$ for arbitrary spin s with the corresponding Clebsch-Gordan coefficients $\langle SM|ik\rangle \equiv \langle SM|s, i, s, k\rangle$. Here g_S denotes the interaction strength for the scattering of two particles with total spin S . For a real spin-3/2 system there are only scattering channels for $S=0, 2$, but in the numerical simulations of (6) we take into account the values of U_{ijkl} for spin 9/2 in the sub-manifold of $i, j, k, l = \pm 3/2, \pm 1/2$, which also depend on $g_{4,6,8}$ [23]. Since in the experiment spin-waves along the z -axis are created, an effective one-dimensional kinetic equation is sufficient to describe these spin-waves. This is obtained by integrating out the transversal degrees of freedom from the three-dimensional case. The coupling constants for the 3D case, $g'_S = \frac{4\pi\hbar^2}{m} a_S$ with s -wave scattering lengths a_S , are modified by the local transversal density profile as $g_S = \frac{\int dx \int dy (n(x, y, z))^2}{(\int dx \int dy n(x, y, z))^2} \times g'_S$. This modification depends on z but only weakly so we approximate it with the central density $n(x, y, 0)$.

Linearized kinetic equation and moment method

Frequencies for small amplitude spin-waves in the linear regime, such as close to the minimum in Fig. 3(a), can be obtained by linearizing the kinetic equation (7). For this, we consider small changes with respect to the stationary state $W_{mn}^0(z, p)$, namely $W_{mn}(z, p, t) = W_{mn}^0(z, p) + \delta W_{mn}(z, p, t)$. Thus we investigate the spin-waves for short times and small amplitudes. The mean-field, as a function of density likewise expands as $V_{mn}(z, t) = V_{mn}^0(z) + \delta V_{mn}(z, t)$ and we substitute both expressions into (6) without the anticommutator, to obtain the linearized kinetic equation

$$(\partial_t - \partial_0) \delta W = \frac{1}{i\hbar} ([\delta W, V^0] + [W^0, \delta V,]) \quad (8)$$

Our next step to explicitly study different kinds of spin-wave modes is the so called *moment method* [43]. The thinking behind it is to look at the time evolution of moments of the position and momentum operators. The l -th moment of such an operator in the phase-space representation is the expectation value

$\langle z^l \rangle_{mn}(t) = \int dp \int dz \delta W_{mn}(z, p, t) z^l$. Expanding the kinetic equation in moments means taking into account only different modes of spin-waves up to a certain order, e.g. dipole (sloshing) modes for $l=1$, quadrupole (breathing) oscillations for $l=2$ and further.

First we need to find a suitable expression for the stationary state $W_{mn}^0(z, p)$, the state of the system before a spin-wave is excited by applying a gradient. With the preparation scheme in mind, considering the preparation pulse to be infinitely short in time, we approximate W_0 as a product of spin and orbital degrees of freedom $W_{mn}^0(z, p) \approx M_{mn} f_0(z, p)$ where M_{mn} is a matrix in spin space determined by the preparation pulses and f_0 is the phase-space distribution for a two-component Fermi gas onto which the pulse is applied. This distribution is given for a non-interacting gas in a harmonic trap in local-density approximation as $f_0(z, p) = \int d^2x \int d^2p (\exp(\beta(\frac{p^2}{2m} + \frac{1}{2}m(\omega_x^2 x^2 + \omega_y^2 y^2 + \omega_z^2 z^2 - \mu)) + 1)^{-1}$. In principle, corrections to this distribution arise due to interactions but in our case the mean-field energy is small compared to kinetic and potential energy and we neglect them. The mean-field $V_{mn}^0(z) = \tilde{M}_{mn} n_0(z)$ then depends on the density distribution $n_0(z) = \int dp f_0(z, p)$, and we introduce the short notation $\tilde{M}_{mn} = \sum_{kl} (U_{klmn} - U_{kmnl}) M_{kl}$. For the frequencies of the dipole modes we expand δW and δV into moments of position and momentum up to first order only

$$\delta W_{mn}(z, p, t) = f_0(z, p) (A_{mn}(t) + z B_{mn}(t) + p C_{mn}(t)) \quad (9)$$

$$\delta V_{mn}(z, p, t) = n_0(z) (\tilde{A}_{mn}(t) + z \tilde{B}_{mn}(t)) . \quad (10)$$

We take the zeroth and first moments of z, p of δW in (9) and obtain their relationship to A, B, C

$$A_{mn} = \frac{1}{N} \langle 1 \rangle_{mn}, B_{mn} = \frac{\langle z \rangle_{mn}}{\langle z^2 \rangle_0}, C_{mn} = \frac{\langle p \rangle_{mn}}{\langle p^2 \rangle_0}, \quad (11)$$

with particle number $N = \int dz \int dp f_0(z, p)$, as well as $\langle z^2 \rangle_0 = \int dz \int dp z^2 f_0(z, p)$ and $\langle p^2 \rangle_0 = \int dz \int dp p^2 f_0(z, p)$. We substitute expressions (11) into the linearized equation (8), then take again the zeroth and first moments of z, p to obtain three equations for the matrices A, B, C respectively

$$\partial_t A = \frac{I_0}{i\hbar} ([M, \tilde{A}] + [A, \tilde{M}]) , \quad (12)$$

$$\partial_t B - m \omega_z^2 C = \frac{I_1}{i\hbar} ([M, \tilde{B}] + [B, \tilde{M}]) , \quad (13)$$

$$\partial_t C + \frac{1}{m} B = \frac{I_2}{i\hbar} [C, \tilde{M}] , \quad (14)$$

with coefficients $I_0 = \frac{1}{N} \int dz n_0(z)^2$, $I_1 = \frac{1}{\langle z^2 \rangle_0} \int dz z n_0(z)^2$ and $I_2 = \frac{1}{\langle p^2 \rangle_0} \int dz \int dp p^2 f_0(z, p) n_0(z)$. The first equation is decoupled from the others and does not lead to

spatial dynamics, so we discard it. Equations (13) and (14) describe dipole oscillations of all spin components of the Wigner function and the frequencies can be obtained by a Fourier transform $\partial_t \rightarrow -i\omega$ and solving the eigenvalue equations, similar to the procedure for a spin 1 Bose gas in Refs. [34, 35].

SU(N) interactions

For the sake of simplicity we now demonstrate this for the special case of SU(N)-symmetry ($N = 2s + 1$) assuming all scattering lengths to be equal. For the $s = 3/2$ subsystem of ^{40}K considered in the experiments, our numerical comparison shows only small differences in the spin-wave behavior between this case and the true scattering parameters. In the SU(4)-symmetric case with all scattering lengths equal, $g_0 = g_2 = \dots \equiv g$, the coupling constants are of the particularly simple form $U_{ijkl} = \frac{g}{2}(\delta_{ij}\delta_{kl} - \delta_{il}\delta_{kj})$. For all matrices with a tilde in equations (12), (13) and (14) we obtain the simple expression $\tilde{M} = g(\text{Tr}(M)\mathbb{1} - M)$. Further, the r. h. s. of Eqs. (12) and (13) are zero and the equations for B, C , written in matrix form reduce to

$$\partial_t B - m\omega_z^2 C = 0 \quad (15)$$

$$\partial_t C + \frac{1}{m}B = \frac{gI_2}{i\hbar}[M, C] \quad (16)$$

which decouple trivially. After a Fourier transform $\partial_t \rightarrow -i\omega$ we obtain the eigenvalue equation

$$(\omega^2 - \omega_z^2)C = 2\omega\omega_{\text{mf}}[M, C] \quad (17)$$

where we have introduced the mean-field frequency $\omega_{\text{mf}} = gI_2/2\hbar$. For all (nematic) initial spin states M considered here the solutions of (17) are either the trivial case $\omega = \pm\omega_z$ that corresponds for instance to oscillations of the entire atomic cloud in the trap or

$$\omega = -\omega_{\text{mf}} \pm \sqrt{\omega_{\text{mf}}^2 + \omega_z^2}. \quad (18)$$

which describe the spin-wave propagation.

S6. TENSOR EXPANSION OF THE WIGNER FUNCTION

The methods described thus far in this supplemental material are valid for any value of the spin. We now focus on the $s = 3/2$ case in order to demonstrate the self-decoupling of the spin-nematic component. In previous studies of the $s = 1/2$ case [37, 38] the kinetic equation and Wigner-function were rewritten in terms of the Pauli matrices $W = \frac{1}{2}(W_0\mathbb{1} + \vec{W} \cdot \vec{\sigma})$ which form a complete basis for Hermitian 2×2 -matrices and allow to identify the vector-part of the mean-field as an effective magnetic

field. For $s = 3/2$ we define a similar basis T_l^m comprising the identity matrix $T_0^0 = \frac{1}{2}\mathbb{1}$, the three spin operators $T_1^m = \frac{1}{\sqrt{3}}S_m$, five quadrupole operators T_2^m and seven octupole operators T_3^m . For the quadrupole we select all traceless symmetric matrices quadratic in \vec{S} ,

$$T_2^0 = \frac{1}{2}\left(S_z^2 - \frac{5}{4}\mathbb{1}\right) \quad (19a)$$

$$T_2^1 = \frac{1}{2\sqrt{3}}(S_x^2 - S_y^2) \quad (19b)$$

$$T_2^2 = \frac{1}{2\sqrt{3}}(S_x S_y + S_y S_x) \quad (19c)$$

$$T_2^3 = \frac{1}{2\sqrt{3}}(S_z S_x + S_x S_z) \quad (19d)$$

$$T_2^4 = \frac{1}{2\sqrt{3}}(S_y S_z + S_z S_y) \quad (19e)$$

and for the octupole

$$T_3^0 = \frac{\sqrt{5}}{3}\left(S_z^3 - \frac{41}{20}S_z\right) \quad (20a)$$

$$T_3^1 = \frac{\sqrt{5}}{3}\left(S_x^3 - \frac{41}{20}S_x\right) \quad (20b)$$

$$T_3^2 = \frac{\sqrt{5}}{3}\left(S_y^3 - \frac{41}{20}S_y\right) \quad (20c)$$

$$T_3^3 = \frac{1}{2\sqrt{3}}\{S_x, S_y^2 - S_z^2\} \quad (20d)$$

$$T_3^4 = \frac{1}{2\sqrt{3}}\{S_y, S_z^2 - S_x^2\} \quad (20e)$$

$$T_3^5 = \frac{1}{2\sqrt{3}}\{S_z, S_x^2 - S_y^2\} \quad (20f)$$

$$T_3^6 = \frac{1}{\sqrt{3}}(S_x S_y S_z + S_z S_y S_x). \quad (20g)$$

This set of 16 Hermitian matrices forms an orthonormal basis set with respect to the trace

$$\text{Tr}(T_l^m T_{l'}^{m'}) = \delta_{ll'} \delta_{mm'}, \quad (21)$$

so we can expand the Wigner function into

$$W(z, p) = \sum_{l=0}^3 \sum_{m=0}^{2l} W_l^m(z, p) T_l^m, \quad (22)$$

with coefficients $W_l^m(z, p) = \text{Tr}(T_l^m W(z, p))$. This expansion is analogous to the *moment method* shown above, but with respect to moments of spin operators. In this basis the coupling constants of the mean-field (7) have the form

$$U_{abcd} - U_{adcb} = \sum_{l=0}^3 \sum_{m=0}^{2l} \alpha_l (T_l^m)_{ab} (T_l^m)_{cd}, \quad (23)$$

where the coefficients α_l depend on the coupling constants g_S . In a real $s = 3/2$ system, $\alpha_1 = \alpha_3$, which is a

result of the $SO(5)$ symmetry of the system [44]. Analogous to (22) the mean-field can be expanded as

$$V(z) = \sum_{l=0}^3 \sum_{m=0}^{2l} V_l^m(z, p) T_l^m, \quad (24)$$

and we find, that in this basis the mean-field is directly proportional to the Wigner function with the coefficients α_l

$$V_l^m(z) = \alpha_l \int dp W_l^m(z, p). \quad (25)$$

We now insert equations (22), (24) and (25) into the kinetic equation (6), neglecting the anticommutator for simplicity and obtain

$$(\partial_t - \partial_0) \sum_{l=0}^3 \sum_{m=0}^{2l} W_l^m(z, p) T_l^m = \frac{1}{i\hbar} \sum_{l', l''} \sum_{m', m''} \alpha_{l''} \int dq W_{l''}^{m''}(z, q) W_{l'}^{m'}(z, p) [T_{l'}^{m'}, T_{l''}^{m''}]. \quad (26)$$

The time evolution for each tensorial component W_l^m of the Wigner function is obtained from (26) by taking the trace with respect to the T_l^m basis as in (21). On the right hand side we define

$$\Lambda_{l'l''l}^{m'm''m} = \text{Tr} \left(T_l^m [T_{l'}^{m'}, T_{l''}^{m''}] \right), \quad (27)$$

such that (26) becomes

$$(\partial_t - \partial_0) W_l^m(z, p) = \frac{1}{i\hbar} \sum_{l', l''} \sum_{m', m''} \alpha_{l''} \int dq W_{l''}^{m''}(z, q) W_{l'}^{m'}(z, p) \Lambda_{l'l''l}^{m'm''m}. \quad (28)$$

Equation (27) simply states the decomposition of the commutators of tensor operators in the tensor basis itself. Apart from the trivial case that T_0^0 commutes with all other tensors we know that by construction $[T_1^i, T_1^j] = i\sqrt{5} \sum_k \epsilon_{ijk} T_1^k$ and thus $\Lambda_{111}^{ijk} = i\sqrt{5} \delta_{l1} \epsilon_{ijk}$. Formulating an explicit expression for all values of $\Lambda_{l'l''l}^{m'm''m}$ is not straightforward so we restrict ourselves to provide those values of l, l', l'' for which the $\Lambda_{l'l''l}^{m'm''m}$ are non-zero for all values of m, m', m'' :

1	(1', 1'')	(29)	
0	(0, 0)		
1	(1, 1), (2, 2), (3, 3)		
2	(1, 2), (2, 1), (2, 3), (3, 2)		
3	(2, 2), (3, 3), (1, 3), (3, 1)		

These relations show, which tensor components l', l'' contribute to the time evolution of the tensor component l .

To illustrate these findings in a matrix representation we introduce the symbolic notation $W_l = \text{Tr}(W T_l) T_l$ suppressing the m -indices, and insert the relations (29) into the equations of motion for W_l . This brings us to equation (2) of the manuscript

$$\begin{aligned} \partial_t W_0 &\cong \partial_0 W_0, \\ \partial_t W_1 &\cong \partial_0 W_1 + \frac{1}{i\hbar} ([W_1, V_1] + [W_2, V_2] + [W_3, V_3]), \\ \partial_t W_2 &\cong \partial_0 W_2 + \frac{1}{i\hbar} ([W_2, V_1 + V_3] + [W_1 + W_3, V_2]), \\ \partial_t W_3 &\cong \partial_0 W_3 + \frac{1}{i\hbar} ([W_3, V_1] + [W_1 + W_3, V_3] + [W_2, V_2]), \end{aligned} \quad (30)$$

where the self-decoupling of the nematic spin tensor is evident, since no term of the form $[W_2, V_2]$ exists on the right hand side of the equation for $\partial_t W_2$.

* Corresponding author: klaus.sengstock@physnet.uni-hamburg.de

- [1] D. Vollhardt, N. Blumer, K. Held, and M. Kollar, *Metallic Ferromagnetism - An Electronic Correlation Phenomenon*, Lecture Notes in Physics **580** (Springer, Heidelberg, Germany, 2001)
- [2] P. A. Lee, N. Nagaosa, and X.-G. Wen, *Rev. Mod. Phys.* **78**, 17 (2006)
- [3] I. Žutić, J. Fabian, and S. Das Sarma, *Rev. Mod. Phys.* **76**, 323 (2004)
- [4] B. R. Johnson, J. S. Denker, N. Bigelow, L. P. Lévy, J. H. Freed, and D. M. Lee, *Phys. Rev. Lett.* **52**, 1508 (1984)
- [5] W. J. Gully, and W. J. Mullin, *Phys. Rev. Lett.* **52**, 1810 (1984)
- [6] E. P. Bashkin, *JETP Lett.* **33**, 8 (1981)
- [7] C. Lhuillier, and F. Lalœ, *J. Physique* **43**, 197 (1982)
- [8] L. P. Lévy, and A. E. Ruckenstein, *Phys. Rev. Lett.* **52**, 1512 (1984)
- [9] J. M. McGuirk, H. J. Lewandowski, D. M. Harber, T. Nikuni, J. E. Williams, and E. A. Cornell, *Phys. Rev. Lett.* **89**, 090402 (2002)
- [10] X. Du, L. Luo, B. Clancy, and J. E. Thomas, *Phys. Rev. Lett.* **101**, 150401 (2008)
- [11] B. DeMarco and D. S. Jin, *Phys. Rev. Lett.* **88**, 040405 (2002)
- [12] C. A. Regal, M. Greiner, and D. S. Jin, *Phys. Rev. Lett.* **92**, 040403 (2004)
- [13] A. Sommer, M. Ku, G. Roati, and M. W. Zwierlein, *Nature* **472**, 201 (2011).
- [14] G. B. Jo, Y. R. Lee, J. H. Choi, C. A. Christensen, T. H. Kim, J. H. Thywissen, D. E. Pritchard, and W. Ketterle, *Science* **325**, 1521-1524 (2009)
- [15] S. Zhang and T. L. Ho, *New J. Phys.* **13**, 055003 (2011)
- [16] G. J. Conduit, and E. Altman, *Phys. Rev. A* **83**, 043618 (2011)
- [17] D. Pekker, M. Babadi, R. Sensarma, N. Zinner, L. Pollet, M. W. Zwierlein, and E. Demler, *Phys. Rev. Lett.* **106**, 050402 (2011)
- [18] T. L. Ho, *Phys. Rev. Lett.* **81**, 742 (1998).

- [19] T. L. Ho and S. Yip, Phys. Rev. Lett. **82**, 247 (1999)
- [20] R. B. Diener, and T. L. Ho, Phys. Rev. Lett. **96**, 190405 (2006)
- [21] R. Barnett, A. Turner, and E. Demler, Phys. Rev. Lett. **97**, 180412 (2006)
- [22] J. Stenger, S. Inouye, D. M. Stamper-Kurn, H.-J. Miesner, A. P. Chikkatur, and W. Ketterle, Nature **396**, 345 (1998)
- [23] J. S. Krauser, J. Heinze, N. Fläschner, S. Götzke, Ole Jürgensen, Dirk-Sören Lühmann, C. Becker, and K. Senstock, Nature Physics **8**, 813 (2012)
- [24] L. E. Sadler, J. M. Higbie, S. R. Leslie, M. Vengalattore, and D. M. Stamper-Kurn, Nature **443**, 312 (2006)
- [25] C. Honerkamp, and W. Hofstetter, Phys. Rev. Lett. **92**, 170403 (2004)
- [26] M. Hermele, V. Gurarie, and A. M. Rey, Phys. Rev. Lett. **103**, 135301 (2009)
- [27] M. A. Cazalilla, A. F. Ho, and M. Ueda, New J. Phys. **11**, 103033 (2009)
- [28] A. V. Gorshkov, M. Hermele, V. Gurarie, C. Xu, P. S. Julienne, J. Ye, P. Zoller, E. Demler, M. D. Lukin, and A. M. Rey, Nature Physics **6**, 289 (2010)
- [29] S. Taie, Y. Takasu, S. Sugawa, R. Yamazaki, T. Tsujimoto, R. Murakami, and Y. Takahashi, Phys. Rev. Lett. **105**, 190401 (2010)
- [30] P. Lecheminant, E. Boulat, and P. Azaria, Phys. Rev. Lett. **95**, 240402 (2005)
- [31] Á. Rapp, G. Zaránd, C. Honerkamp, and W. Hofstetter, Phys. Rev. Lett. **98**, 160405 (2007)
- [32] C. Wu, Mod. Phys. Lett. B **20**, 1707 (2006), and references therein
- [33] K. Rodriguez, A. Argüelles, M. Colome-Tatche, T. Vekua, and L. Santos, Phys. Rev. Lett. **105**, 050402 (2010)
- [34] Y. Endo, and T. Nikuni, J. Low Temp. Phys. **152**, 21-46 (2008)
- [35] S. S. Natu, and E. J. Mueller, Phys. Rev. A **81**, 053617 (2010)
- [36] See online supplemental material for details on the quantum gas preparation, detection and data analysis, as well as in-depth discussion of the theoretical model, the method of moments and the tensor decomposition.
- [37] U. Ebling, A. Eckardt, and M. Lewenstein, Phys. Rev. A **84**, 063607 (2011)
- [38] J. N. Fuchs, D. M. Gangardt, and F. Laloë, Eur. Phys. J. D **25**, 57 (2003)
- [39] S. S. Natu, and E. J. Mueller, Phys. Rev. A **79**, 051601(R) (2009)
- [40] F. Piéchon, J. N. Fuchs, and F. Laloë, Phys. Rev. Lett. **102**, 215301 (2009)
- [41] The equation is depicted symbolically. For an explicit derivation see [36].
- [42] J. M. McGuirk and L.F. Zajiczek, N. J. Phys. **12**, 103020 (2010)
- [43] T. Nikuni, J. E. Williams, and C. W. Clark, Phys. Rev. A **66**, 043411 (2002)
- [44] C. Wu, J. P. Hu, and S. C. Zhang, Phys. Rev. Lett. **91**, 186402 (2003)